

# The Yang-Mills spectrum from a 2-level algorithm

Harvey B. Meyer

Theoretical Physics, University of Oxford, 1 Keble Road,  
Oxford, OX1 3NP, United Kingdom

meyer@thphys.ox.ac.uk

**Abstract.-** We investigate in detail a 2-level algorithm for the computation of 2-point functions of fuzzy Wilson loops in lattice gauge theory. Its performance and the optimization of its parameters are described in the context of 2+1D  $SU(2)$  gluodynamics. In realistic calculations of glueball masses, it is found that the reduction in CPU time for given error bars on the correlator at time-separation  $\sim 0.2\text{fm}$ , where a mass-plateau sets in, varies between 1.5 and 7 for the lightest glueballs in the non-trivial symmetry channels; only for the lightest glueball is the 2-level algorithm not helpful. For the heavier states, or for larger time-separations, the gain increases as expected exponentially in  $mt$ . We present further physics applications in 2+1 and 3+1 dimensions and for different gauge groups that confirm these conclusions.

# 1 Introduction

The study of pure gauge theories on the lattice at zero temperature has now been for a few years in an era of precision “numerical experiments”. Highlights of the latter include the determination of the low-lying glueball spectrum in 2+1 [1] and 3+1 [2] dimensions, the confining string spectrum ([3] and [4]) as well as ratios of stable string tensions in  $SU(N)$  gauge theories ([5], [6]). The reasons for this progress lie both in the increase in computing power and in the development of new numerical techniques, such as the fuzzing procedures ([7] and [8]), improved actions (e.g. [2]) and multi-level algorithms (MLA) ([9], [10] and [11]). The purpose of this paper is to investigate the performance of the version proposed in [11].

Retrospectively, we consider that the first multi-level algorithm was proposed in [9]; it bears the name of the “multihit method”, and consists in replacing the link variables by their average under fixed nearest-neighbour links, when computing a Wilson or Polyakov loop. It is a realisation of the real-space renormalisation group transformation. Only much more recently was it realised [10] that - thanks to the locality property - the idea can be applied more generally and iteratively by performing nested averages under fixed boundary conditions (BC). Multi-level algorithms are of course particularly powerful in theories with a mass gap, where distant regions of the lattice are almost uncorrelated. An impressive increase in the performance with respect to the ordinary 1-level algorithm was achieved in the Polyakov loop correlator - the improvement is proportional to the area span by the two loops. A further step towards generalization was taken in [11], where the algorithm was adapted to any functional of the links - including fuzzy operators - that can be factorized. Indeed the factors need not even be gauge-invariant. The efficiency of the algorithm is based on the fact that the UV fluctuations can be averaged out separately for each factor, effectively achieving  $n^{n_f}$  measurements by only actually computing  $n$  of them, where  $n$  is the number of measurements done at the lower level of the algorithm and  $n_f$  the number of factors. The choice of the factorization is thus dictated by a competition between having as many factors as possible and each factor being as independent of the BC as possible.

In glueball and string tension calculations, the smearing [7] and blocking [8] techniques, used in conjunction with the variational method [23], have become part of the well-established machinery to efficiently determine the glueball spectrum. Such fuzzy operators have typically large overlaps onto the fundamental state in the studied symmetry channel and are far less sensitive to UV fluctuations than bare Wilson loops. While it is clear that for asymptotically large Euclidean time separation, the multi-level algo-

rithm becomes more efficient than the 1-level algorithm, the question of real practical interest is whether one can truly improve the efficiency of realistic calculations. Typically, the operators have reached mass plateaux already at 0.2fm in the case of glueballs. In such a regime, one cannot expect a statistical error reduction by orders of magnitude. Only a numerical analysis can reliably address the question formulated above.

It is equally important to determine whether the efficiency of the algorithm is maintained as the lattice spacing is decreased. Indeed the correlation length becomes larger and larger in lattice units and one might wonder whether the low-level measurements at fixed BCs are still helping to reduce the dominant fluctuations on the correlator.

The outline of this paper is as follows. After a description of the algorithm (section 2), we investigate in section 3 the dependence of the 2-level algorithm on its parameters in the context of glueball 2-point function calculations. We numerically demonstrate (section 4) that the parameters of the algorithm can easily be optimized and compare its efficiency to that of the 1-level algorithm as the continuum is approached. Special attention is paid to the operators bearing vacuum quantum numbers, for which the vacuum expectation value (VEV) must be subtracted carefully. In section 5, we present miscellaneous physics applications (glueballs and  $k$ -strings in 2+1 and 3+1 dimensions). We end with a summary and an outlook on possible future developments. The appendix contains a comment on the Lüscher-Weisz algorithm.

## 2 Algorithm description

In this section, we describe the implementation of a 2-level algorithm for the measurement of 2-point correlation functions. We use the isotropic Wilson action, and the update is done with compounds sweeps consisting of a 1+3 mixture of heat-bath [21] and over-relaxation [22] sweeps.

The operators are smeared, blocked, definite-momentum operators in 2+1 dimensional  $SU(2)$  gauge theory. We shall use glueball operators as examples, however the conclusions will be shown in subsequent sections to be applicable to the measurement of fuzzy spatial flux-tubes as well.

The details of the algorithm [11] are the following. The lattice size is  $N_x \times N_y \times N_t$ . After a number  $N_{up}$  of compound update sweeps, we freeze  $N_t/\Delta$  time-slices separated by distance  $\Delta$ , and measure the average values  $\langle \mathcal{O}(t_i) \rangle_{bc}$  of the operators in all the other time-slices  $t_i$  between the fixed time-slices by doing  $n$  updates under these fixed BCs. These average values in each time-slice are kept separately. They are written to disk before updating the full lattice again.  $N_{up}$  is typically chosen to be  $n/10$ , so as

to represent a negligible amount of computer time, and nevertheless ensure good statistical independence of the “compound measurements” (this will be checked in section 4).

After  $N_{bc}$  of these compound measurements, the correlator for  $t \geq 2a$  can then easily be computed ‘off-line’ from

$$\langle \mathcal{O}(t_i) \mathcal{O}(t_j) \rangle = \frac{1}{N_{bc}} \sum_{bc} \langle \mathcal{O}(t_i) \rangle_{bc} \langle \mathcal{O}(t_j) \rangle_{bc}, \quad (1)$$

if the time-slices  $t_i$  and  $t_j$  do not belong to the same “time-block”. This equation holds because the BCs have been generated with the weighting given by the full lattice action [10].

A few comments on the data storage are in order. If  $N_{op}$  are being measured, the amount of data generated is

$$\text{nb(data)}_{\text{II}} = N_{op} \times N_t \times N_{bc}.$$

This is to be contrasted with the ordinary way of storing the data: the correlation matrix is computed during the simulation, and stored in typically  $N_{bin} = \mathcal{O}(100)$ :

$$\text{nb(data)}_{\text{I}} \simeq N_{op}^2 \times N_t \times N_{bin}.$$

The ratio is thus

$$\frac{\text{nb(data)}_{\text{II}}}{\text{nb(data)}_{\text{I}}} = \frac{1}{N_{op}} \frac{N_{bc}}{N_{bin}} \quad (2)$$

As an example, for a large production run with a total of  $10^6$  measurements, we may do  $n = 10^3$  measurements under  $N_{bc} = 10^3$  fixed BCs. Therefore, for  $N_{op} \gg 10$  - which is usually the case -, the data size is smaller than with the 1-level algorithm. The obvious advantage of version II is that one can use a much larger number of operators (e.g. include non-zero momenta, scattering states, the square of the traces of operators, ...). Further advantages include:

- one can choose the binning *a posteriori*, thus making a more detailed check of auto-correlations possible;
- if e.g.  $\Delta = 8$  and one is computing the 2-point function at  $t = 5$ , there are several ways to obtain it, which of course all have the same average, but different variances; it is very convenient to be able to choose which combination is optimal *a posteriori* (see section 5).
- in principle, one can extract 3- and 4-point function from the same data set, as long as one correlates operators that have been averaged in different time-blocks. Derivatives of the 2-point function can be computed just as easily.

On the other hand a downside of this way of proceeding is that one loses information on the short-range correlator (0 and 1 lattice spacing of Euclidean time separation). The time-zero correlator is useful because it allows one to evaluate the overlap of the original operators onto the physical states. In some cases it may be desirable to store the BC-averages of the short-range correlators since

$$\langle \mathcal{O}(t_i) \mathcal{O}(t_j) \rangle = \frac{1}{N_{bc}} \sum_{bc} \langle \mathcal{O}(t_i) \mathcal{O}(t_j) \rangle_{bc} \quad (3)$$

if the time-slices  $t_i$  and  $t_j$  belong to the same time-block. Incidentally, for  $t_i = t_j$ , we shall see in section 4 that this measurement can be useful to predict the performance of the algorithm for the larger time-separations.

### 3 The algorithm and its parameters

We now present data obtained at  $\beta = 12$ ,  $V = 32^3$  in the 2+1D  $SU(2)$  pure gauge theory. Note that  $\sqrt{\sigma}a = 0.1179(5)$  [1], which means that  $a = 0.0555\text{fm}$  (if we use  $\sqrt{\sigma} = 420\text{MeV}$ ) and we are indeed well in the scaling region, as far as the low-energy observables are concerned.

We perform a check of the auto-correlation of compound measurements done at fixed BCs. We then proceed to a study of the efficiency of the algorithm as a function of its various parameters: first, the width  $\Delta$  of the time-block inside which the submeasurements are made; secondly, the number of submeasurements. We will then look at the dependence of the error bars on the mass of the state being measured.

**Binning analysis** On fig. 1, we show the error bar on the correlator and its local-effective mass (LEM) for an operator lying in the  $A_2$  irreducible representation (IR, containing spins  $0^-, 4, 8, 12, \dots$ ) as function of the number of jackknife bins. We note that as long as the number of bins is not much smaller than 100, the error bars are stable under the change of binnings. Obviously the error bars are subject to fluctuations themselves, and in some cases we will give estimates of the latter. However we can draw the lesson that the number of updates  $N_{up} \simeq n/10$  is apparently sufficient to decorrelate the BCs sufficiently.

**The distance between fixed boundary conditions** Fig. 2 show the dependence of the error bar on the  $A_2$  correlator as a function of the number of submeasurements  $n$ , at roughly fixed CPU time. We consider that the comparison of error bars is meaningful at the 20% level. The fundamental

state in that lattice IR is relatively heavy and known [13] to have rotation properties very similar to a continuum spin 4 glueball. The left graph shows the  $\Delta = 4$  data, the right one the  $\Delta = 8$  data.

In the first case, the smallest error bar is achieved for the smallest number of measurements (here  $n = 100$ ) for all time-separations ( $t = 2, 3, 4$ ). On the right-hand side, the situation is the following: for time-separations  $t = 2, 3, 4$ , a small number of submeasurements ( $n = 200$ ) is more favourable, while, interestingly, the error bar for the  $t = 5$  correlator is practically independent of  $n$ . For  $t \geq 6$ , the hierarchy is inverted: the runs with a large number of subsweeps ( $n = 800, 1600$ ) yield smaller error bars. This is consistent with the rule of thumb proposed in [11], namely that the optimal number of submeasurements should be of order  $e^{mt}$ . In the present case, this evaluates to  $\sim 1300$ , given that  $am(A_2) \simeq 1.2$ .

We can already draw the conclusion that  $\Delta = 4$  is too small a time block and a significant number of submeasurements does not lead to further variance reduction on the correlator.  $\Delta = 8 \simeq \frac{1}{\sqrt{\sigma a}} \simeq 0.5\text{fm}/a$  on the other hand seems well suited for that purpose. This conclusion is expected to hold also in 3+1D pure gauge systems, since their long distance correlations are very similar to the present 2+1D case.

It is also interesting to look at the error bars on the LEM. Indeed, when a large number of submeasurements is performed, the 2-pt function at time  $t$  and  $t + a$  can be expected to be numerically more strongly correlated, thus leading to reduction of fluctuation of their ratio. This point is illustrated in fig. 2. On the left (concerning  $\Delta = 4$ ), the variance on the LEM at 3.5 lattice spacings is practically constant. On the right, we observe that even at the smaller time separations  $t = 2, 3, 4$ , the runs with a large number of subsweeps (800) are at least as good as the runs with the smaller number of subsweeps (200). From 5.5 onwards, there is a clear advantage at performing a large number of subsweeps. For instance, the error bar for the  $n = 800$  run is roughly 3 times smaller than that for the  $n = 200$  run, and this at equal CPU time.

**Time-separation dependence of the error bars** It is also instructive to look at the same data from another point of view: for a fixed number of submeasurements, how does the error bar on the correlator and on its LEM vary as a function of time separation? On fig. 3, it is clearly seen that the error bar decreases exponentially as the operators are measured further away from the fixed boundaries. For  $\Delta = 8$ , the variance drops by a factor 100 between  $t = 2$  and  $t = 7$  for the runs with  $n = 800$  and 1600.

**Mass dependence of the error bars** We plot the LEM as well as the local decay constant of the error bar on the correlator together on fig. 4. The upper figure illustrates the situation with a large number of submeasurements ( $n = 1600$ ), while the lower shows what happens with only  $n = 200$ .

We show two light states, the fundamental  $A_1$  and  $A_3$  states as well as the fundamental  $A_2$  that was considered up to here. For the  $A_1$  and  $A_3$ , the error bar decays along with the signal, since the former's decay constant matches the LEM of the corresponding operator. As a consequence, long mass plateaux are seen, with error bars increasing only very slowly. For the heavier  $A_2$  state, the error bar decay constant keeps up only to 4.5 lattice spacings, resulting in a fast loss of the signal beyond that. It is nevertheless much more favourable a situation than with only 200 submeasurements: while the lightest glueball plateau is obtained just as well, the  $A_3$  data is much more shaky and the  $A_2$  is essentially lost beyond 4.5 lattice spacings. We note that although the basis of  $A_3$  operators was the same for  $n = 1600$  as for  $n = 200$ , the variational calculation performed slightly less well in the latter case.

In fact, the time separation where the error bar decay constant falls off on fig. 4 gives us an idea of the time-separation for which the number of submeasurements is optimal. Indeed, if the error bar continues to fall off, it means that the measurements have a large degree of statistical dependence through the common BC, since moving further away from the fixed BC makes them less dependent. However, once – far away from the BC – the error bar is constant (i.e. its decay constant is now zero), the signal to noise ratio is falling exponentially to zero. Thus  $n = 1600$  is best suited for measuring the  $A_2$  mass ( $am \simeq 1.2$ ) at 5.5 lattice spacings.

## 4 Optimization procedure & performance

We now proceed to a more systematic study of the efficiency of the 2-level algorithm. We shall consider three states, in the  $A_1$ ,  $A_2$  and  $A_3$  lattice IRs. The lightest states in these representations correspond [13] to the  $J^P = 0^+$ ,  $J = 4$  and  $J = 2$  continuum states. The procedure we adopt is to measure these three correlators at fixed physical Euclidean time separation  $t$ . We do so at three values of  $\beta = 6, 9$  and  $12$  – recall that in the scaling region, the lattice spacing simply scales as  $1/\beta$ . The correlator is evaluated for different numbers of submeasurements under fixed BCs:

$$1 \leq n \leq 200 \tag{4}$$

We then plot the inverse efficiency  $\xi^{-1}$  as a function of the number of submeasurements:

$$\xi^{-1}(n) \equiv [\Delta C_n(t)]^2 \times n, \quad (5)$$

where  $\Delta C_n(t)$  is the error bar on the correlator when measured  $n$  times under fixed BCs. In some cases, we shall also consider the efficiency with respect to the LEM, in which case  $\Delta C_n(t)$  is replaced by  $\Delta m_n^{(\text{eff})}(t)$ .

In this study the number of BCs was 100. They are separated by 80 sweeps. The individual measurements done under fixed BC were stored separately, to allow us to combine them in different ways. In particular, to obtain the efficiency corresponding to 10 submeasurements, for each BC we can split the 200 submeasurements into 20 'independent' sequences of 10 submeasurements. These 20 sequences are then used to estimate the variance on the error bars themselves. On fig. 5, 6 and 7 we show these roughly estimated variances for  $n \leq 20$ , after what the number of 'independent' sequences becomes smaller than 10 and these variance estimates become unreliable. The aim here is only to give the order of magnitude of the uncertainty on  $\xi$ , so as to be able to reach meaningful conclusions concerning its minimum as a function of  $n$ .

Eventually of course it is desirable to have an easier way to optimize the parameters of the algorithms. When we have an operator with exactly vanishing vacuum expectation value (VEV), we define a quantity  $\omega$  as the zero-time-separation correlator, multiplied by the number of submeasurements  $n$ :

$$\omega(n, t_i) = \frac{1}{N_{bc}} \sum_{bc} \sum_{\text{meas}=1}^n \langle \mathcal{O}(t_i)^2 \rangle_{bc} \quad (6)$$

Obviously  $\omega$  is a function of the distance between the time-slice where the operator is measured and the fixed time-slices. It is easy to evaluate this quantity accurately: one of the objectives of this analysis is to check for the validity of this quantity as a predictor of the optimal number of submeasurements of the 2-level algorithm. The absolute value of  $\omega$  will not interest us, rather we will check whether its minimum is reached at the same  $n$  as  $\xi^{-1}(n)$ .

It is also interesting to compare the efficiency of the 2-level algorithm to the standard 1-level algorithm with an equal number of measurements. In this case the translational invariance in the time direction is not broken by the algorithm. The sweeps between BCs have no *raison d'être* here; on the other hand the measurements are done in each time-slice, including those that are kept fixed in the 2-level algorithm. Thus the comparison of algorithms is fair.

Let us first consider the lightest  $A_3$  state (fig. 5). The graphs correspond, from top to bottom to  $\beta = 6, 9$  and 12. We keep the physical time separation

approximately fixed at about 0.22fm (2, 3, and 4 lattice spacings respectively), and similarly the separation of the fixed time-slices is augmented in lattice units ( $4a$  at  $\beta = 6$ ,  $6a$  at  $\beta = 9$  and  $8a$  at  $\beta = 12$ ; we also show the case  $\Delta = 4a$  at  $\beta = 12$  for comparison). The first observation is that the 2-level algorithm performs better at all three lattice spacings. If the number of submeasurements is chosen 'reasonably', the inverse efficiency is smaller by a factor  $\sim 3$  at the coarsest lattice spacing, and by a factor  $\sim 2$  at both of the smaller lattice spacings, provided  $\Delta$  is kept fixed in physical units. Secondly, the curve for  $\xi^{-1}$  is extremely flat around its minimum. For instance, at  $\beta = 9$  it seems that it does not matter whether one does 10 or 40 submeasurements, the performance for this particular observable will be unchanged. The flatness becomes even more pronounced closer to the continuum. This however is not true for the case  $\Delta = 4a$  at  $\beta = 12$ . Although the curve has a narrow minimum at a small number of submeasurements, the efficiency then decreases rapidly and this setup becomes less favourable than the standard algorithm. Thirdly, we note that the quantity  $\omega$  shown at  $\beta = 12$  (it has been rescaled in such a way that it can be plotted along with the other curves) is a very good predictor of the minimum of the inverse efficiency curve  $\xi^{-1}$ , and this both when  $\Delta = 4a$  and  $\Delta = 8a$ . Its qualitative aspect (including the flatness) is very similar to the  $\xi$  curve.

The qualitative statements that have been made for the  $A_3$  correlator also apply to the  $A_2$  correlator (see fig. 6), whose mass is larger by a factor  $\sim 4/3$ . As one might expect, the higher mass favours the use of the 2-level algorithm even more: the gain in CPU time for constant error bars is roughly a factor 6 at all three values of  $\beta$ . Again the  $\xi$  curve is extremely flat, but the optimal number of submeasurements has shifted to the right: in fact, 100 submeasurements seems to be a good choice at all three lattice spacings. Choosing a narrow width for the time-blocks has the clear disadvantage of leading to a smaller gain in efficiency and that this efficiency varies much more rapidly with the number of submeasurements. These facts are again well predicted by the curve  $\omega$ .

**The  $0^{++}$  case** We now move to the  $A_1$  correlator, which gives the mass of the lightest glueball. Since this is the trivial representation, the operator has a non-zero VEV, which has to be subtracted in one way or the other in order to extract information on the glueball spectrum. With the ordinary 1-level algorithm, it is customary to subtract the VEV *a posteriori*:

$$C(t) = \sum_{t'} \langle (\mathcal{O}(t') - \langle \mathcal{O} \rangle) (\mathcal{O}(t+t') - \langle \mathcal{O} \rangle) \rangle$$

$$\equiv \sum_{t'=1}^{N_t} \langle \mathcal{O}(t') \mathcal{O}(t+t') \rangle - \frac{1}{N_t} \left( \sum_{t'=1}^{N_t} \langle \mathcal{O}(t') \rangle \right)^2 \quad (7)$$

This way of proceeding is perfectly applicable to the 2-level algorithm, *provided that only those measurements incorporated in the 2-point function are included in the VEV evaluation*. In other words, exactly the same measurements must appear in the second sum as in the first in eqn. 7:

$$C(t) = \sum_{t' \in \Theta_t} \langle \mathcal{O}(t') \mathcal{O}(t+t') \rangle - \frac{1}{\#(\Theta_t)} \left( \sum_{t' \in \Theta_t} \langle \mathcal{O}(t') \rangle \right)^2 \quad (8)$$

where  $\Theta_t$  is a subset of  $\{1, \dots, N_t\}$ . It varies with  $t$ : depending the time-separation, the measurement of the correlator uses different time-slices. It is recommended to store the measurements in double precision, since the cancellation between the two sums grows with the time-separation.

Our experience is that failing to do the subtraction in this way leads to a very large variance on the correlator (typically 30 – 50% in a typical run). The explanation is that in this way, one is really measuring, on a large but finite set of configurations, the fluctuation of the operator around its average value *measured on these configurations*. Naturally, in the infinite statistics limit, both schemes give the same answer, but the proposed one benefits from the strong correlation between the 2-point and 1-point function when they are measured on the same configurations.

There are of course many alternative possibilities<sup>1</sup>. One of them relies on the variational method [23], which is widely used to improve the projection onto the fundamental state and to extract information on the excited spectrum. It was applied for instance in [13] and consists in feeding the *unsubtracted* correlation matrices into the variational calculation. The generalized eigenvalue problem then yields the massless vacuum, followed by the fundamental glueball, the first excited, etc. The determination of the vacuum is very accurate in our experience, and the variance on the masses of the physical states did not seem to be higher. Naturally, one of the operators in the basis is wasted to project out the vacuum, but this is not an issue when one disposes of a large set of operators, as is usually the case.

Finally, we note that another group [14] has used the 2-level algorithm for compact  $U(1)$  scalar glueball calculations, where the forward-backward symmetric derivative of the correlator was taken. It is clear that at small temporal lattice spacing, the finite-difference formula can evaluate the derivative accurately, due to the large correlations between time-slices. The idea is thus related to that expressed by eqn. 8.

---

<sup>1</sup>I thank Urs Wenger for discussions on this point.

These different methods are illustrated on fig. 7: the inverse efficiency of the 1- and 2-level algorithms are plotted as a function of  $n$ . The VEV has been subtracted either by use of eqn. 8 or by applying the variational method to a set of three operators (the resulting operator had very large overlap onto the lightest state in either method, and therefore a comparison is meaningful). We see that with either algorithm, the two VEV-subtraction methods perform equally well. The second observation is that the 2-level algorithm is performing poorly here, if  $n \geq 10$ . If we turn to the LEM, we see that both the derivative-method and the direct VEV-subtraction method have the same efficiency, once the number of measurements for  $n \geq \mathcal{O}(50)$ . For  $n \leq 50$ , the VEV-subtraction looks better; note however that, for discretization reasons, the LEM on the derivative is actually at 4 lattice spacings, rather than 3.5.

## 5 Physics applications

We present four datasets: glueballs and  $k$ -string tensions in 2+1 and 3+1 dimensions. We shall be comparing the efficiency of the ordinary 1-level algorithm with the 2-level algorithm. A general comment applies to all four cases: the operators used are all variationnally [23] determined linear combinations of smeared [7], blocked [8] operators which large overlaps onto the physical states. The variational method involves Cholesky-decomposing a correlation matrix, which fails if the statistical noise spoils the positivity of the matrix. Our experience with the 1-level algorithm is that the procedure often fails for that reason if it is applied at  $t \geq 1$ . By contrast, we were always able to perform the decomposition when using the 2-level algorithm. The explanation is that the operators decaying more rapidly, which couple to excited states, are more accurately measured in such a way that the positivity is preserved.

### 5.1 Glueballs in 2+1 dimensions

As a first physics application of the methods that have been presented, we extract the masses of several excited-glueball masses in 2+1D  $SU(2)$  gluodynamics. Table 6 shows the data at three different lattice spacings. The parameters of the 2-level algorithm are  $n = 5000, 1000, 800$  and  $\Delta = 4, 6, 8$  respectively for  $\beta = 6, 9, 12$ . The variational method is applied at 2.5 lattice spacings for the first two lattice spacings, and 3.5 lattice spacings for the third. A detailed efficiency comparison has already been made in section 4. The identification of the continuum numbers was worked out in [13] and [12], and will be further detailed elsewhere [19], but we now dispose of increased statistics and make use of the 2-level algorithm: this allows us to

obtain an accurate determination of glueball masses as heavy as three times the lightest glueball. In the future this ability will have to be followed by the development of techniques to reduce systematic uncertainties on glueball spectroscopy measurements (mixing of single-glueball states with scattering states, multi-torelon states, ...).

## 5.2 Glueballs in 3+1 dimensions

The multi-level algorithm applied to gauge-invariant correlators was first tested on glueball operators in the 3+1 dimensional  $SU(3)$  gauge theory [11]. Some exploratory steps were carried out to optimize the parameters, while in this paper we have performed a much more detailed study in 2+1 dimensions. One might wonder whether the conclusions carry over to 3+1 dimensions, since the short-distance fluctuations scale differently.

Here we shall simply present a comparison of efficiency in a realistic case of glueball calculations at  $\beta = 6.0$ ,  $\beta = 6.2$  and  $\beta = 6.4$ , where we can compare our data to that of the 10-year-old UKQCD data [24]. The parameters of the 2-level algorithm are  $n = 40$  for all three values of  $\beta$ , while  $\Delta = 8$  for  $\beta = 6.2$  and  $6.4$ , and  $\Delta = 6$  for  $\beta = 6.0$ . Let us focus on the lightest states in the  $A_1^{++}$ ,  $E^{++}$  and  $T_1^{++}$  representations (see table 2). We compare the efficiency in terms of the error bars on the LEMs by scaling the 1-level error bar to the number of sweeps done in the run where the 2-level algorithm was implemented (see eqn. 5). The same conclusions hold than in 2+1D: apart from the lightest glueball, the efficiency of the 2-level algorithm is greater than that of the 1-level one, and increases rapidly with the mass of the state. The comparison to the UKQCD data is slightly less robust, because the operators used are not the same. The difference in the extent of the time direction was compensated by scaling up the statistics of the 2-level run. Nevertheless, the same trend is observed as in the comparisons at the coarser lattice spacings.

Consider the correlator at four lattice spacings. It can be obtained by correlating the time slices situated symmetrically around the fixed time-slice, or asymmetrically. Naturally, the first way is more favourable. However, for a very massive state, the measurements are expected to be very weakly correlated to the fixed BC; therefore the asymmetric correlator can increase the statistics and reduce the final error bar. In fact, one can make any mixture of both measurements. If  $\bar{t}$  is the time-coordinate of the fixed BC:

$$\begin{aligned}
C(t=4) &\propto \frac{\alpha}{N_{bc}} \sum_{bc} [\mathcal{O}(\bar{t}+1)\mathcal{O}(\bar{t}-3) + \mathcal{O}(\bar{t}-1)\mathcal{O}(\bar{t}+3)] \\
&+ \frac{1}{N_{bc}} \sum_{bc} \mathcal{O}(\bar{t}+2)\mathcal{O}(\bar{t}-2)
\end{aligned} \tag{9}$$

The parameter  $\alpha$  can be optimized as well. This is illustrated on fig. 8, where the variances of the LEMs are plotted as a function of  $\alpha$  for  $\beta = 6.0$ . We see that the optimal value of  $\alpha$  increases with the mass of the state, as one might expect. However, the dependence on  $\alpha$  is weak for  $\alpha \geq 0.2$ : choosing  $\alpha = 0.3$  is practically optimal for all states and  $\alpha = 1$  is not much worse (note that the choice of  $\alpha$  is done *a posteriori*).

### 5.3 $k$ -strings in 2+1 dimensions

We present an excerpt of a dataset that will be published in full elsewhere [25]. We compute masses of  $k = 1, 2, 3$  and 4 fuzzy flux tubes in 2+1D  $SU(8)$  gauge theory; our methodology follows that of [6]. Table 3 contains data obtained both with the 1- and 2-level algorithms on a relatively coarse lattice ( $\sqrt{\sigma}a = 0.2550(4)$ ). The algorithm parameters are  $n = 1000$ ,  $\Delta = 4$ . It was anisotropic in size in order to check for corrections to the linear dependence of the mass on the length of the Polyakov loop.

The small mass of the  $k = 1$ ,  $L \simeq 2\text{fm}$  state makes the 1-level far more efficient to compute the LEM even at 2.5 lattice spacings. The 2-level algorithm only becomes superior for  $L \geq 2.6\text{fm}$ . Another point is that the overlap of our operator onto the fundamental state is better than 99%, which means that the mass can be extracted already at 0.5 lattice spacings. The lesson we learn from this is that it is worth keeping the correlator at small time-separations, as indicated in section 2.

For all other states, the conclusions are quite different: the 2-level algorithm is 4 times more efficient for the  $k = 2$   $L = 2\text{fm}$  string, and this gain in efficiency grows extremely rapidly with the mass of the state.

### 5.4 $k$ -strings in 3+1 dimensions

Finally, we present data obtained some time ago on  $k = 1$  and  $k = 2$  strings in 3+1D  $SU(4)$  gauge theory at three different lattice spacings (see table 4). For  $\beta = 10.90, 11.10, 11.50$ , the parameters of the 2-level algorithm were  $n = 80, 20, 20$  and  $\Delta = 6, 4, 4$  respectively. The masses are extracted from cosh fits starting at 2.5 lattice spacings. The data at the first two values of  $\beta$  can be directly compared to that of [6], where  $10^5$  sweeps were done in each case with the 1-level algorithm. Two comments are in order: the  $k = 1$  string is more accurately obtained with the 1-level algorithm, while the 2-level algorithm performs slightly better for the  $k = 2$  string at  $\beta = 11.10$ , although its parameters may not have been optimal. At  $\beta = 10.90$ , we notice a discrepancy between the two masses of 2.9 standard deviations. This is presumably due to the fact that the cosh fit was started

at one lattice spacing [18] for that particular state in the work of Teper and Lucini. Generally speaking, the 2-level algorithm has the advantage of yielding longer mass plateaux because of the decrease of the error bar with the separation to the BC, and therefore helps reducing the systematic error. Indeed lattice calculations, because of the positivity property of correlators, naturally tend to overestimate the masses extracted from them.

## 6 Summary & outlook

It is time to summarize what we have learnt about the 2-level algorithm. We have emphasized the linear dependence of the data size on the number of operators; auto-correlations can be checked for easily, and the precise way in which the correlator is computed can be optimized *a posteriori*.

The optimization study of the parameters led to the conclusion that  $\Delta \simeq \frac{1}{\sqrt{\sigma a}}$  is a good choice for the separation of the fixed time-slices. In that case, the variance of the correlator decreases exponentially  $\sim e^{-mt}$  as long as the number of measurements at fixed boundary conditions  $n > e^{mt}$ . As a consequence, longer mass plateaux are seen, even for the more massive states. This feature should help in reducing the systematic bias to overestimate the masses being calculated.

Suppose we want to compute the correlator at time-separation  $t$  from measurements in time-slices  $\bar{t} + t/2$  and  $\bar{t} - t/2$  with respect to the fixed time-slice position  $\bar{t}$ . The optimization of  $n$  can be achieved by minimizing [the  $t = 0$  correlator measured  $n$  times at distance  $t/2$  from fixed time-slices]  $\times n$ . This is an easy quantity to compute as function of  $n$ ; it is sufficient to store the individual measurements separately. For a fixed physical separation  $t$ , the optimal number of measurements  $n$  is only weakly dependent on the lattice spacing. A possibility that we have not explored is to let the number of measurements depend on the boundary conditions, with a termination condition determined by the desired accuracy (which would presumably be chosen to be proportional to  $1/\sqrt{N_{bc}}$ ).

The efficiency of the 2-level algorithm was compared to that of the 1-level algorithm in 2+1 and 3+1 dimensions for various gauge groups. We found that the 2-level algorithm performs better for all glueball states but the lightest. The kind of gain in computing-time one can expect in realistic glueball spectrum calculations varies between 1.5 and 7 for the lightest states in the lattice irreducible representations in the case of 2+1D  $SU(2)$ . The gain then increases exponentially with the mass of the state. If high accuracy is required for the lightest glueball, it might make sense to do a separate run using the 1-level algorithm: at any rate, it will use far less computing

time than is required for the heavy states. The same qualitative statements apply in computations of flux-tube masses. The 2-level algorithm starts to become more favourable at a string length of  $\sim 2.5\text{fm}$ ; and it is always more performant for the excited states and the strings of higher representations.

We would like to conclude by mentioning two further applications of the 2-level algorithm. As was suggested in [11], the method should be well suited to compute 3-point functions of glueballs [15] and flux-tubes [16], since these observables involve 3 factors, each subject to UV fluctuations. The possibility is being investigated.

An alternative to variational calculations in conjunction with a large number of fuzzy operators is the spectral function method (for a review, see [17]) in conjunction with the maximal entropy method to perform the inverse Laplace transform. It would be interesting to investigate the possibility of using UV operators (e.g. a bare plaquette, which couples equally to many states) to extract the glueball spectrum. The correlator would need to be measured very accurately – and here we expect the 2-level algorithm to be of great help – on a lattice with a very fine temporal resolution. We leave this line of research open for the future.

**Acknowledgements** In the course of this work I benefited a lot from interacting with Biagio Lucini, Michael Teper and Urs Wenger at Oxford University. I also thank M. Hasenbusch, S. Kratochvila, P. Majumdar and P. Weisz for interesting discussions at LATTICE 03. The numerical calculations were performed on PPARC and EPSRC funded workstations and on a Beowulf cluster in Oxford Theoretical Physics. Finally I wish to thank the Berrow Trust for financial support.

## References

- [1] M. J. Teper, Phys. Rev. D **59** (1999) 014512 [arXiv:hep-lat/9804008].
- [2] C. J. Morningstar and M. J. Peardon, Phys. Rev. D **60** (1999) 034509 [arXiv:hep-lat/9901004].
- [3] M. Luscher and P. Weisz, JHEP **0207** (2002) 049 [arXiv:hep-lat/0207003].
- [4] K. J. Juge, J. Kuti and C. Morningstar, arXiv:hep-lat/0312019.
- [5] L. Del Debbio, H. Panagopoulos, P. Rossi and E. Vicari, JHEP **0201** (2002) 009 [arXiv:hep-th/0111090].

- [6] B. Lucini and M. Teper, Phys. Rev. D **64** (2001) 105019 [arXiv:hep-lat/0107007].
- [7] M. Albanese *et al.* [APE Collaboration], Phys. Lett. B **192** (1987) 163.
- [8] M. Teper, Phys. Lett. B **183** (1987) 345.
- [9] G. Parisi, R. Petronzio and F. Rapuano, Phys. Lett. B **128** (1983) 418.
- [10] M. Luscher and P. Weisz, JHEP **0109** (2001) 010 [arXiv:hep-lat/0108014].
- [11] H. B. Meyer, JHEP **0301** (2003) 048 [arXiv:hep-lat/0209145].
- [12] H. B. Meyer and M. J. Teper, Nucl. Phys. B **658** (2003) 113 [arXiv:hep-lat/0212026].
- [13] H. B. Meyer and M. J. Teper, Nucl. Phys. B **668** (2003) 111 [arXiv:hep-lat/0306019].
- [14] P. Majumdar, Y. Koma and M. Koma, arXiv:hep-lat/0309038.
- [15] G. A. Tickle and C. Michael, Nucl. Phys. B **333** (1990) 593.
- [16] P. Pennanen, A. M. Green and C. Michael, Phys. Rev. D **56** (1997) 3903 [arXiv:hep-lat/9705033].
- [17] M. Asakawa, T. Hatsuda and Y. Nakahara, Prog. Part. Nucl. Phys. **46** (2001) 459 [arXiv:hep-lat/0011040].
- [18] M. Teper, private communication
- [19] H.B. Meyer, D.Phil. thesis, in preparation
- [20] N. Cabibbo, E. Marinari, Phys. Lett. B **119**(1982) 387
- [21] K. Fabricius, O. Haan, Phys. Lett B **143** (1984) 459;  
A.D. Kennedy, B.J. Pendleton, Phys. Lett., **156B** (1985) 393
- [22] S.L. Adler, Phys. Rev. D **23** (1981) 2901
- [23] B. Berg and A. Billoire, Nucl. Phys. B **221** (1983) 109.  
M. Lüscher, U. Wolff, Nucl. Phys. B **339** (1990) 222.
- [24] G. S. Bali, K. Schilling, A. Hulsebos, A. C. Irving, C. Michael and P. W. Stephenson [UKQCD Collaboration], Phys. Lett. B **309** (1993) 378 [arXiv:hep-lat/9304012].

- [25] H.B. Meyer, C.P. Korthals Altes, in preparation
- [26] P. Weisz, private communication (Tsukuba, Jul. 2003)
- [27] M. Hasenbusch, private communication (Tsukuba, Jul. 2003)
- [28] M. Laine, H.B. Meyer, K. Rummukainen, M. Shaposhnikov, in preparation

## Comment on the Lüscher-Weisz algorithm

Consider the LW algorithm for bare time-like Polyakov loop correlators. It was noted by several groups ([26], [27], [28] (where the implementation is due to K. Rummukainen)) that the LW algorithm can probably still be improved (and also simplified) for large enough separation  $R$ .

Indeed the physical system consisting of one “time block” with fixed spatial links as BC can be studied for itself. It is reminiscent of the finite-temperature gauge system, where the BC are however periodic. The two systems have the same exact  $Z_N$  symmetry which can be broken spontaneously if the width of the block is small (corresponding to high temperature). It must thus be ensured that this does not happen, otherwise the error reduction will fail to take place: the VEV taken by the segments of Polyakov loop will only be averaged out at the outer level, and will therefore suffer from  $\mathcal{O}(1/\sqrt{N_{bc}})$  fluctuations.

The BCs break Lorentz invariance in the subsystem. However, by analogy with Dirichlet BCs, we expect that the dimensionally-reduced theory, containing a adjoint Higgs field and the gauge field, exhibits a pseudo-mass gap. In this situation, the correlation between the two segments of link products decays very rapidly at large distance  $R$  and it should help to perform multiple measurements of the two segments separately by keeping a slice  $S$  between them fixed. In this way it is not necessary to store the direct product of  $SU(N)$  matrices. In fact, this version of MLA has been found to perform well even in the presence of an adjoint field ([28]).

IR	spin	$\beta = 6.0$	$\beta = 9.0$	$\beta = 12.0$	continuum:
		$a\sqrt{\sigma} = 0.2538(10)$ 10 <sup>7</sup> sweeps	$a\sqrt{\sigma} = 0.1616(6)$ 3 · 10 <sup>6</sup> sweeps	$a\sqrt{\sigma} = 0.1179(5)$ 3 · 10 <sup>6</sup> sweeps	$m/\sqrt{\sigma}$
$A_2$	4	2.423(34)	1.5766(96)	1.183(16)	10.01(16)
	4	2.638(85)	1.804(42)	1.395(57)	11.91(45)
	4	2.89(11)	1.856(86)	1.468(77)	12.22(69)
	4	3.01(15)	2.199(44)	1.698(44)	14.98(49)
$E$	3	2.552(70)	1.663(23)	1.2587(51)	10.84(14)
	1	2.558(43)	1.813(20)	1.360(13)	11.95(18)
	3	2.718(63)	1.855(28)	1.350(23)	11.78(27)

Table 1: The lightest states in the  $A_2$  and  $E$  lattice irreducible representations. The string tension values are taken from [1]. For 2+1D  $SU(2)$  on  $16^3$ ,  $24^3$  and  $32^3$  lattices respectively for the three values of  $\beta$ .

$\beta = 6.0$	$m_{\text{eff}}^{1\text{-lev}}(2.5a)$	$m_{\text{eff}}^{2\text{-lev}}(2.5a)$	$\frac{\xi_{2\text{-level}}}{\xi_{1\text{-level}}}$
$16^3 \times 36$	$4.16 \cdot 10^5$ sweeps	$15.04 \cdot 10^5$ sweeps	
$A_1^{++}$	0.7106(87)	0.7248(55)	0.69
$E^{++}$	1.078(16)	1.0776(63)	1.80
$T_1^{++}$	1.605(90)	1.612(18)	6.55

$\beta = 6.2$	$m_{\text{eff}}^{1\text{-lev}}(3.5a)$	$m_{\text{eff}}^{2\text{-lev}}(3.5a)$	$\frac{\xi_{2\text{-level}}}{\xi_{1\text{-level}}}$
$24^3 \times 32$	$2 \cdot 10^5$ sweeps	$9.28 \cdot 10^5$ sweeps	
$A_1^{++}$	0.531(12)	0.5273(62)	0.83
$E^{++}$	0.768(22)	0.7819(64)	2.46
$T_1^{++}$	0.99(15)	1.250(27)	6.60
$\beta = 6.2$	$m_{\text{eff}}^{1\text{-lev}}(2.5a)$	$m_{\text{eff}}^{2\text{-lev}}(2.5a)$	$\frac{\xi_{2\text{-level}}}{\xi_{1\text{-level}}}$
$24^3 \times 32$	$2 \cdot 10^5$ sweeps	$9.28 \cdot 10^5$ sweeps	
$A_1^{++}$	0.5269(77)	0.5369(52)	0.48
$E^{++}$	0.8079(99)	0.8026(43)	1.12
$T_1^{++}$	1.260(39)	1.294(11)	2.31

$\beta = 6.4$	$m_{\text{eff}}^{\text{UKQCD}}(2.5a)$ [24]	$m_{\text{eff}}^{2\text{-lev}}(2.5a)$	$\frac{\xi_{2\text{-level}}}{\xi_{1\text{-level}}}$
	$V = 32^4: 0.322 \cdot 10^5$ sw	$V = 32^3 \times 48: 1.11 \cdot 10^5$ sw	
$A_1^{++}$	0.415(14)	0.4000(73)	0.64
$E^{++}$	0.620(17)	0.5894(72)	1.08
$T_1^{++}$	1.06(8)	0.946(10)	12.4

Table 2: Comparison of local effective masses using the ordinary 1-level and the 2-level algorithms in 3+1D  $SU(3)$ . The ratios of efficiencies  $\xi$ , representing the inverse ratio of CPU time required for fixed accuracy, is given in the last column. In the last case, the statistics of the 2-level run were scaled up by 1.5 in the efficiency computation to take the different volume into account.

string length	state	$m_{\text{eff}}(1.5a)$	$m_{\text{eff}}(2.5a)$	$m_{\text{eff}}^{2\text{-level}}(2.5a)$	$\frac{\xi_{2\text{-level}}}{\xi_{1\text{-level}}}$
		1-level: $1.2 \cdot 10^5$ sweeps		$16 \cdot 10^5$ sweeps	
$L = 16$	$k = 1$	1.0130(82)	1.001(21)	1.003(16)	0.13
	$k = 2$	1.739(37)	1.74(22)	1.729(30)	4.0
	$k = 3$	2.24(10)	/	2.216(66)	/
	$k = 4$	2.63(25)	/	2.32(12)	/
$L = 20$	$k = 1$	1.292(17)	1.359(66)	1.288(19)	0.90
	$k = 2$	2.27(11)	1.92(77)	2.174(59)	13
	$k = 3$	2.63(27)	/	2.53(23)	/
	$k = 4$	3.01(72)	/	3.04(33)	/

Table 3: The 4  $k$ -string tensions in 2+1D  $SU(8)$  gauge theory,  $V = 16 \times 20 \times 24$ ,  $\beta = 115.0$ , measured with two different algorithms ( $n = 1000$ ,  $\Delta = 4$  for the 2-level case).

state	$\beta = 10.90$ $L = 12$ $1.7 \cdot 10^5$ sweeps	$\beta = 11.10$ $L = 16$ $0.83 \cdot 10^5$ sweeps	$\beta = 11.50$ $L = 24$ $3.6 \cdot 10^5$ sweeps
$am_1$	0.610(19)	0.592(13)	0.4638(71)
$am_1^*$	0.728(75)	0.700(25)	0.680(20)
$am_2$	0.823(25)	0.820(17)	0.616(16)
$am_2^*$	1.187(81)	0.991(56)	0.913(35)
$\sigma_1 a^2$	0.0581(18)	0.04109(90)	0.02114(32)
$\sigma_2 a^2$	0.0759(23)	0.0553(11)	0.02748(71)
$\sigma_2/\sigma_1$	1.306(56)	1.346(40)	1.300(39)

Table 4: The masses of  $k = 1$  and  $k = 2$  strings for 3+1D  $SU(4)$  gauge theory; the string tensions are computed assuming the Lüscher correction  $m = \sigma L - \frac{\pi}{3L}$ , and in the error bar on the ratio  $\sigma_2/\sigma_1$  statistical independence is assumed.

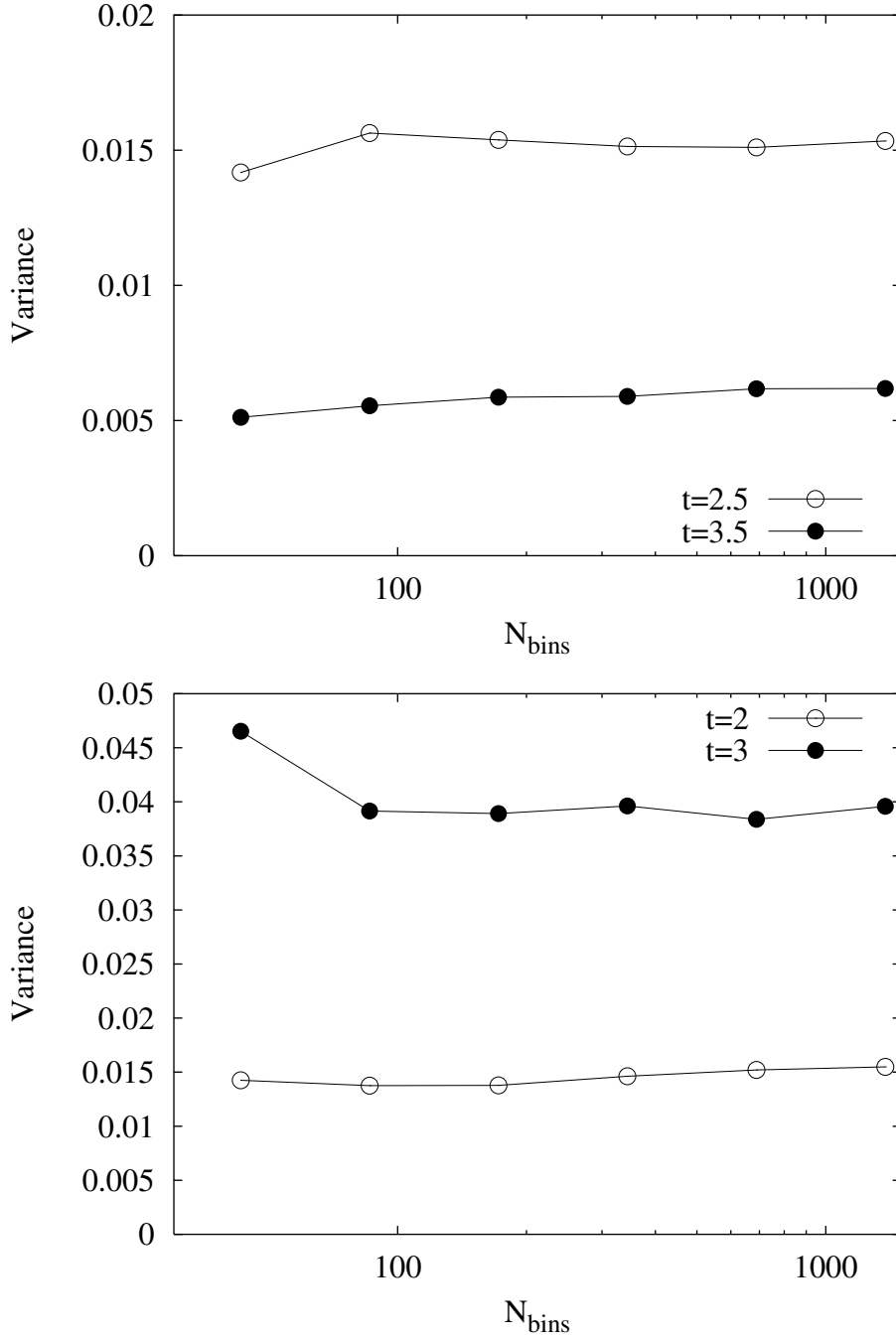


Figure 1: Jackknife-bin-size dependence of the statistical error on the  $A_2$  correlator (top) and its local-effective-mass (bottom). The separation of the fixed time-slices is  $\Delta = 4$ . For 2+1D  $SU(2)$ , at  $\beta = 12$ ,  $V = 32^3$  and  $n = 100$ ,  $N_{bc} = 1400$ .

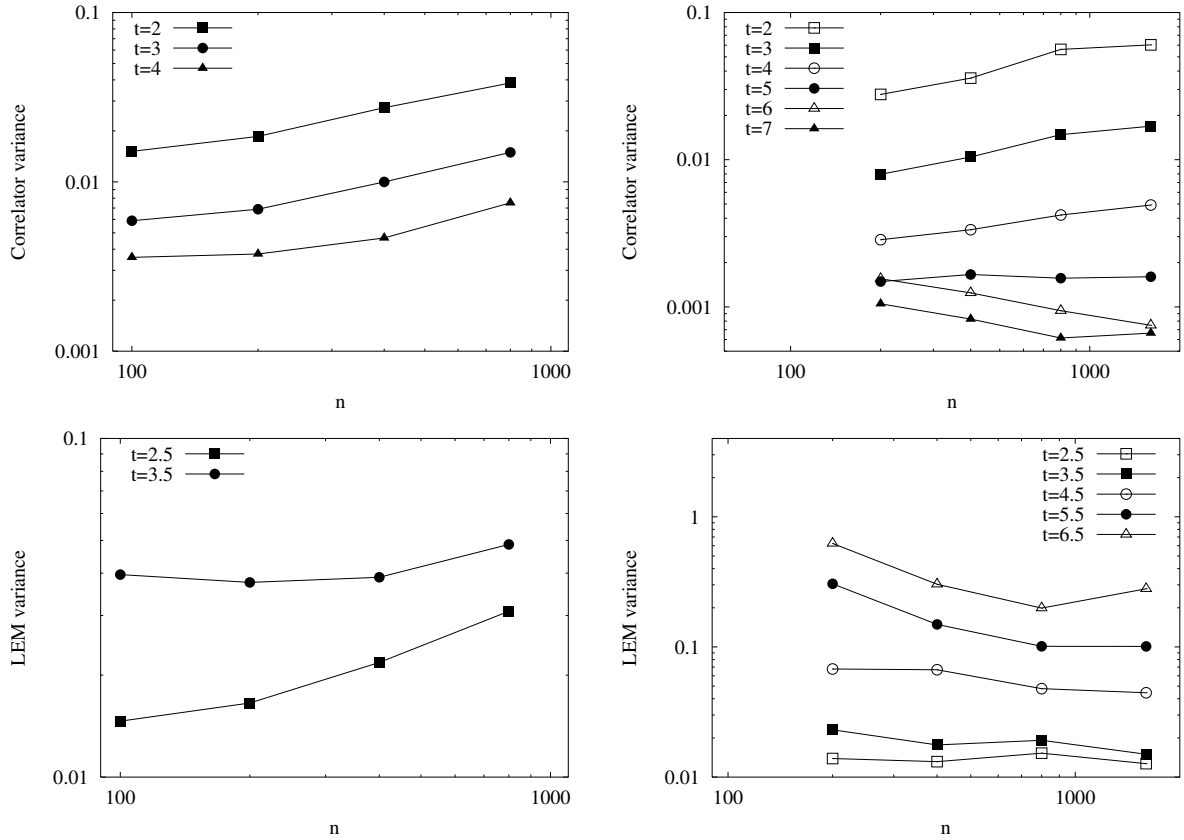


Figure 2: The variance of the correlator (top) and the local effective mass (bottom), as function of the number of measurements under fixed boundary conditions  $n$ , for fixed computing time. The separation of the fixed time-slices is  $\Delta = 4$  on the left and  $\Delta = 8$  on the right. The operator is a linear combination of fuzzy magnetic Wilson loops lying in the  $A_2$  square lattice irreducible representation. For 2+1D  $SU(2)$ , at  $\beta = 12$ ,  $V = 32^3$ .

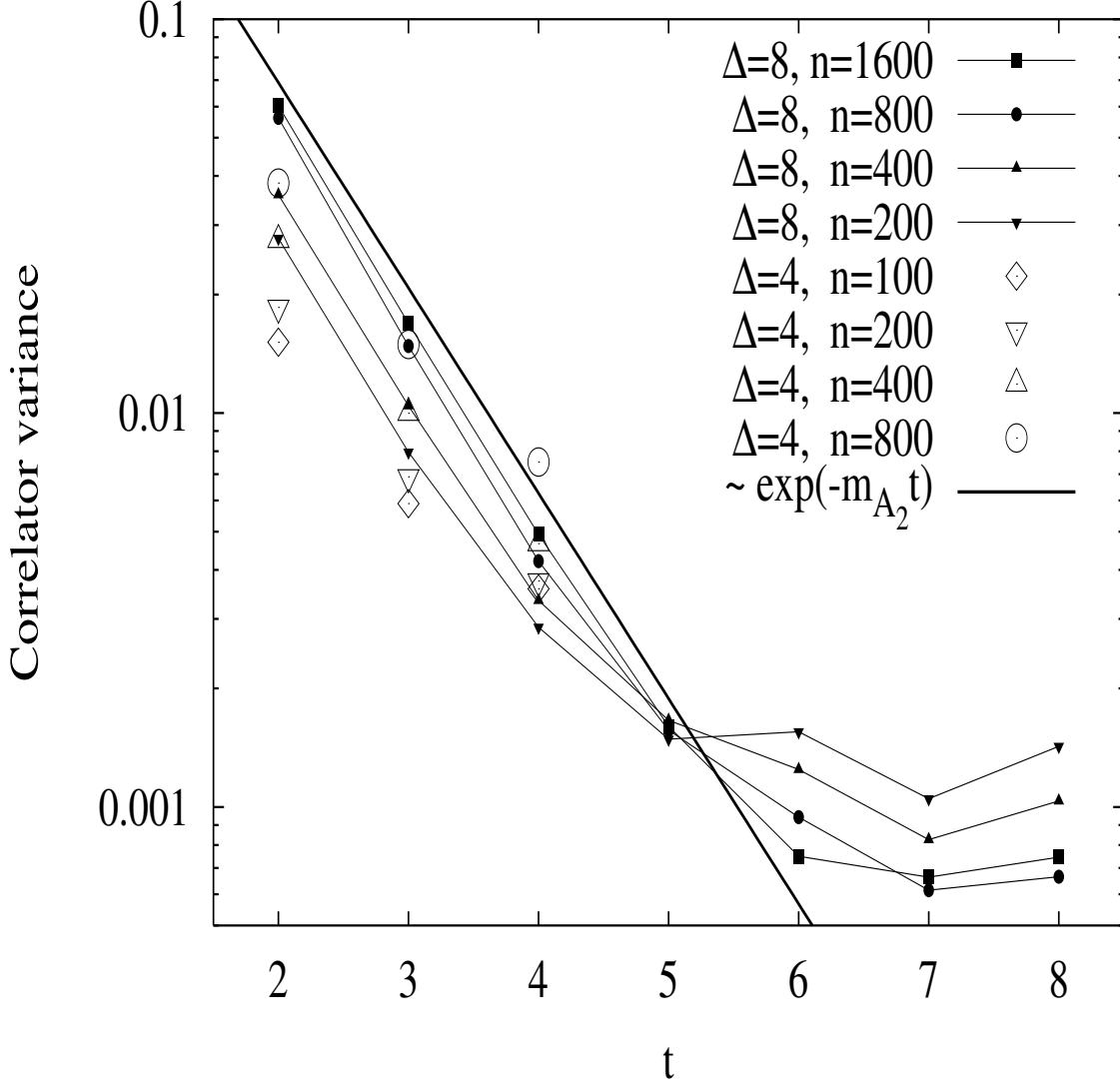


Figure 3:  $A_2$ -correlator variance as function of the Euclidean-time separation  $t$ , for different numbers of measurements under fixed boundary conditions  $n$  and separation of the fixed time-slices  $\Delta$ . The computing time is the same for all points. For 2+1D  $SU(2)$ , at  $\beta = 12$ ,  $V = 32^3$ .

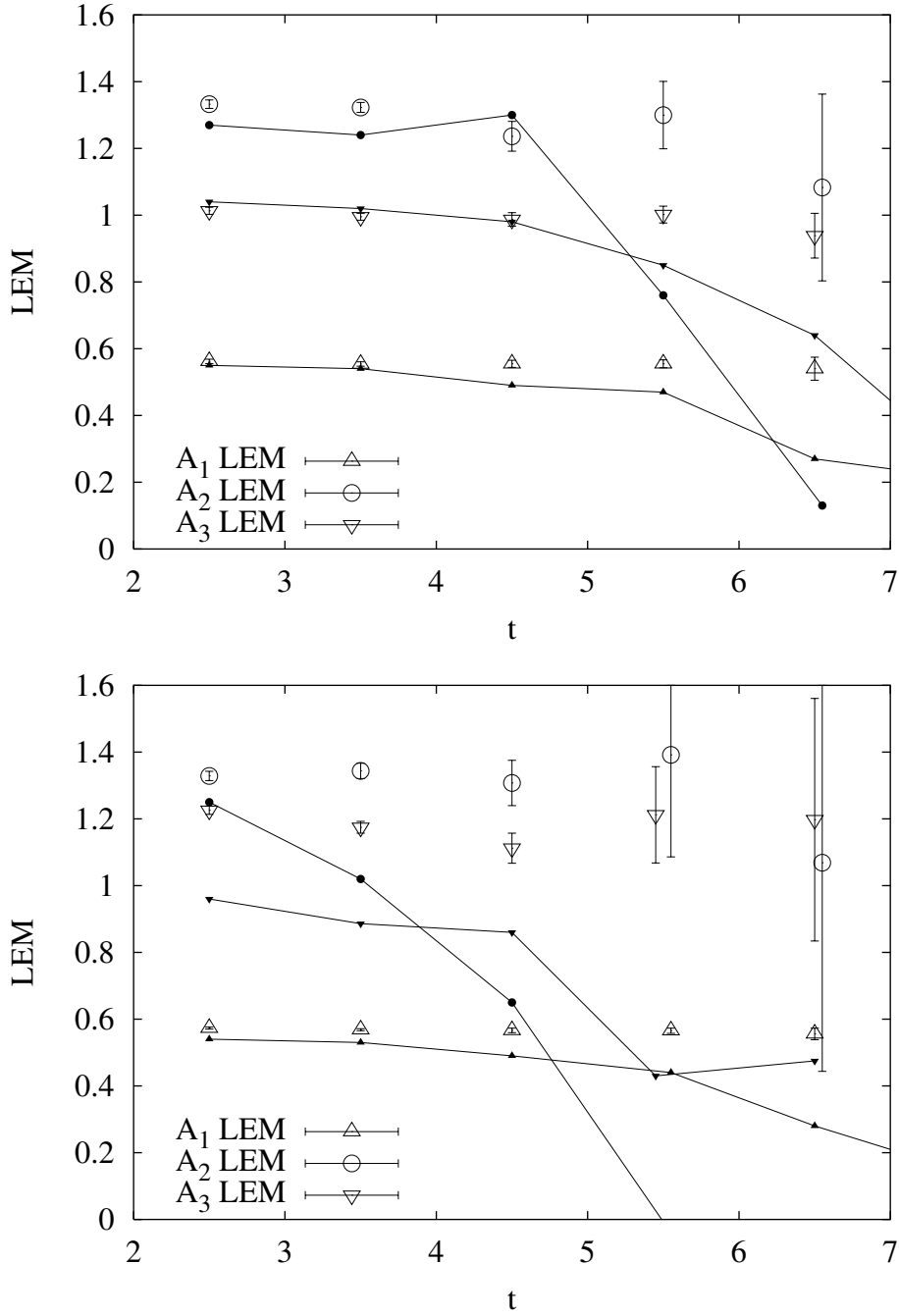


Figure 4: The local-effective-mass of various correlators, and of the variance on the latter, as function of the Euclidean-time separation  $t$ . The distance between fixed time-slices is  $\Delta = 8$  and the number of measurements under fixed boundary conditions is  $n = 1600$  for the top plot and  $n = 200$  for the bottom plot. For 2+1D  $SU(2)$ , at  $\beta = 12$ ,  $V = 32^3$ .

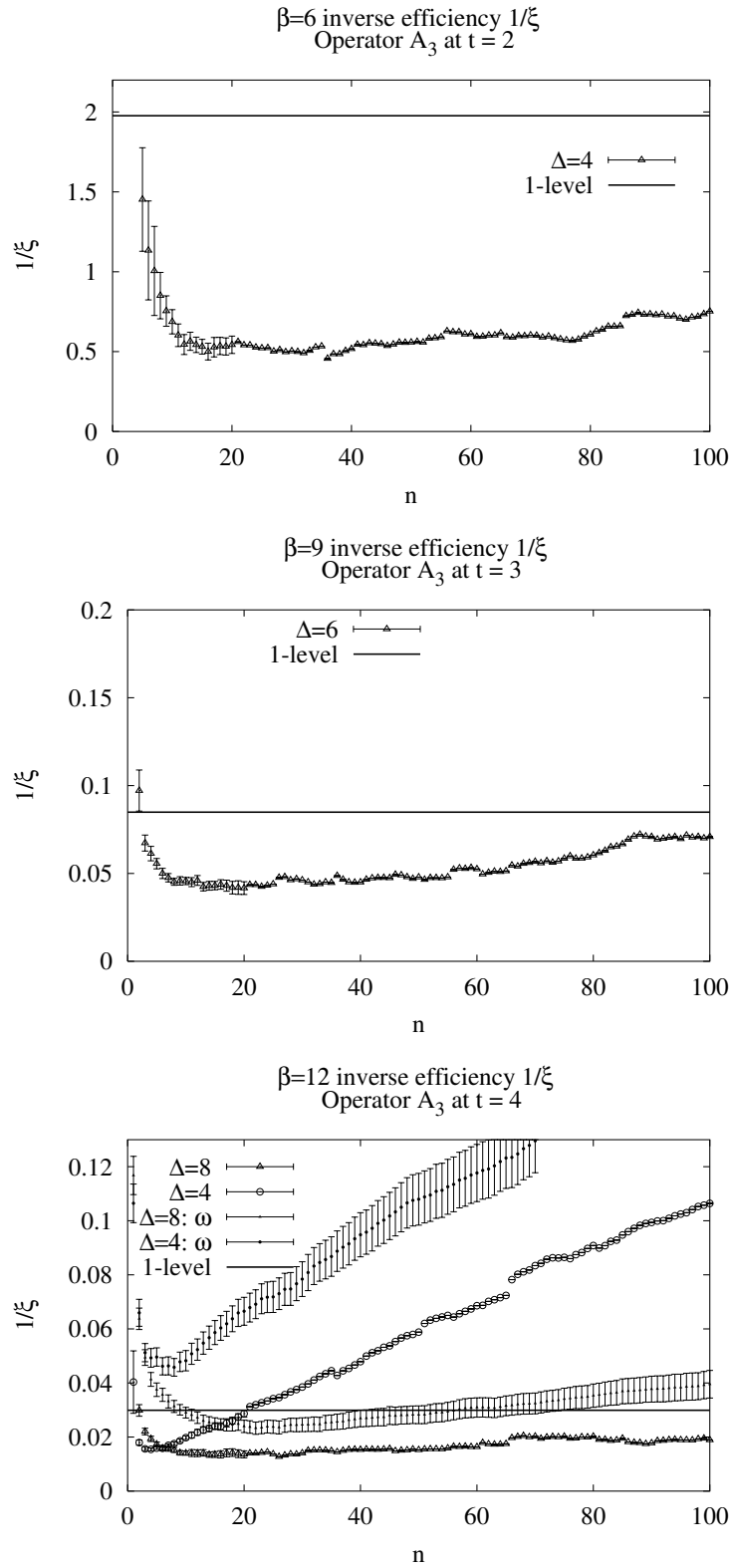


Figure 5:  $A_3$  inverse efficiency and its predictor  $\omega$  in 2+1D  $SU(2)$ .

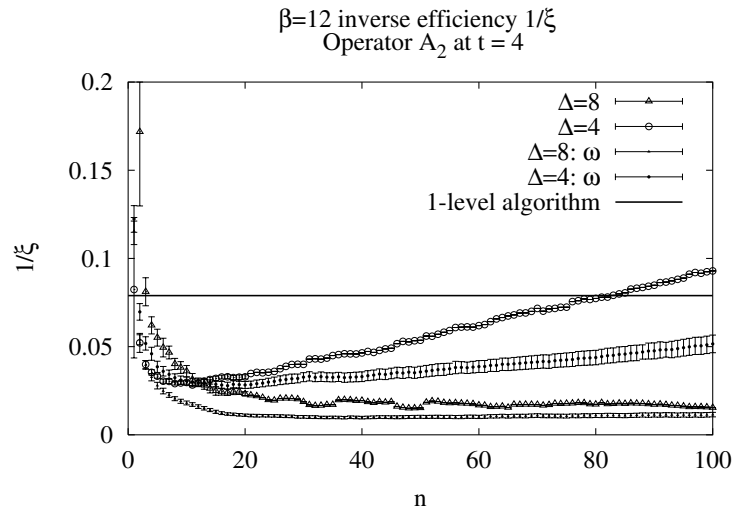
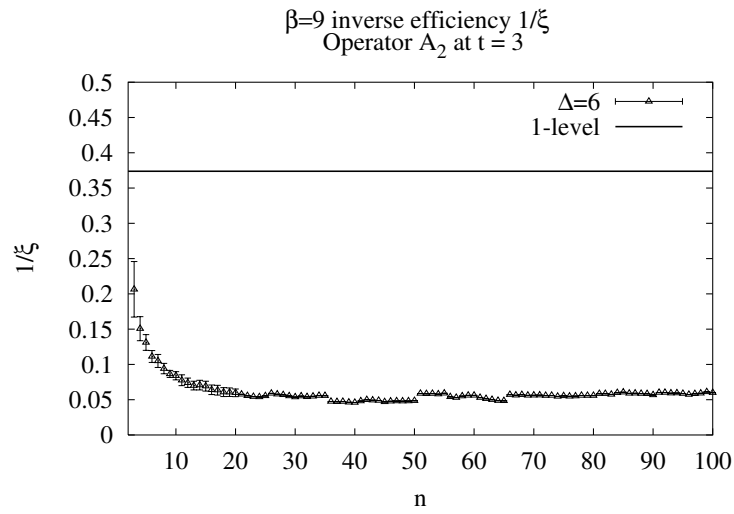
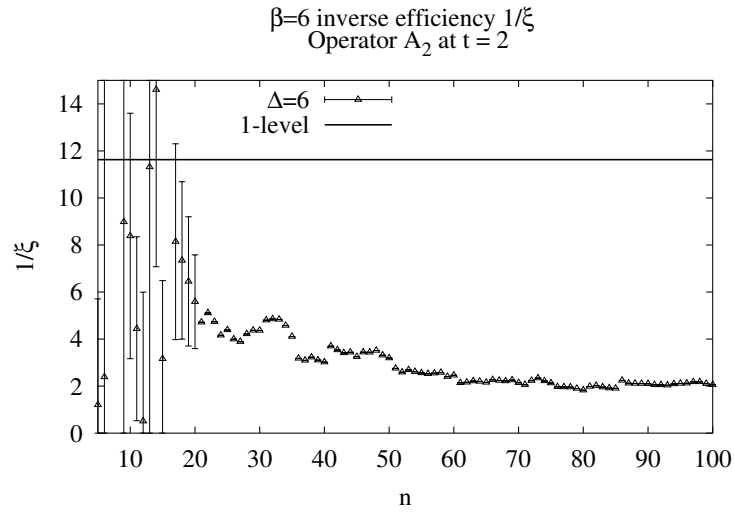


Figure 6:  $A_2$  inverse efficiency and its predictor  $\omega$  in 2+1D  $SU(2)$ .

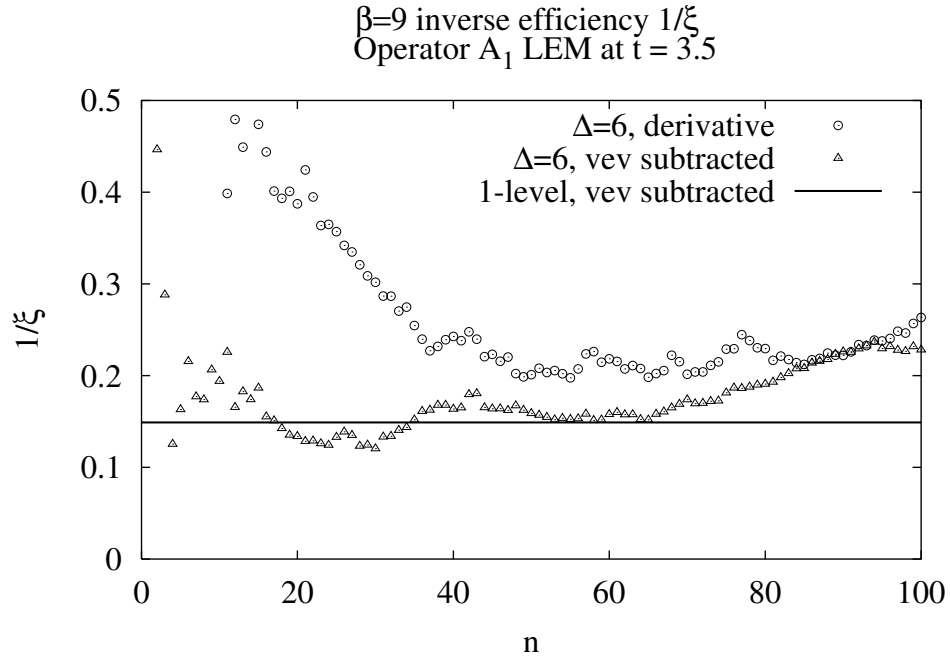
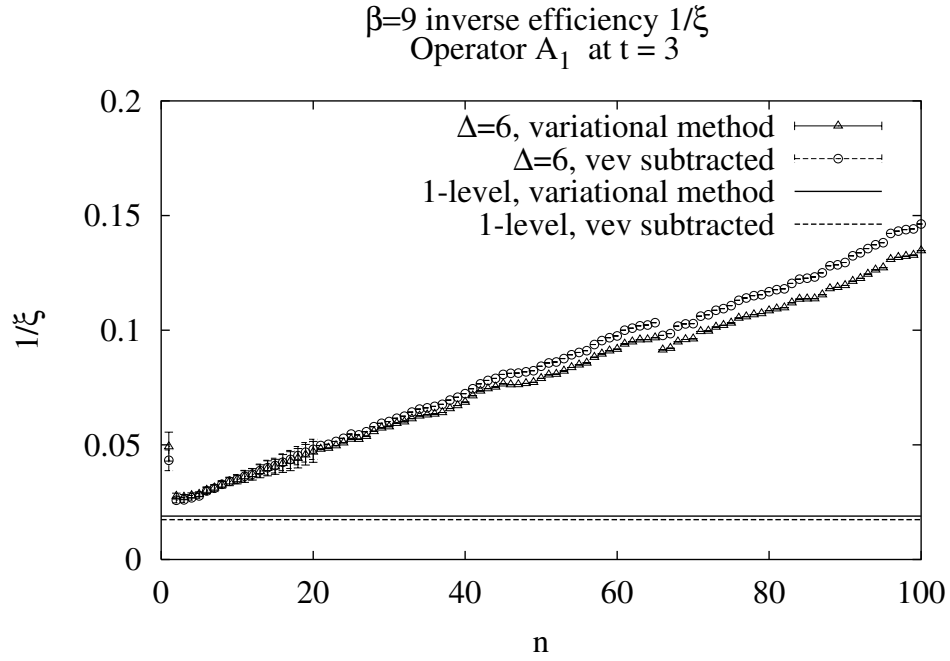


Figure 7:  $A_1$  correlator (top) and LEM (bottom) efficiency curves using various methods of VEV subtraction. In 2+1D  $SU(2)$ .

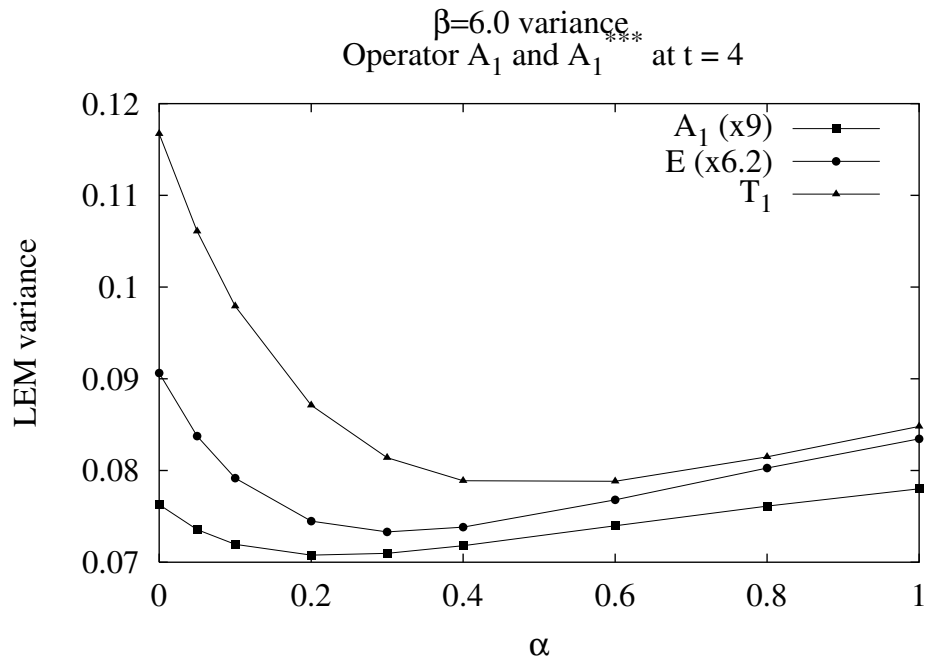


Figure 8: Local-effective-mass variance for three different states, as a function of the weighting parameter  $\alpha$  (cf. section 4). The  $A_1$  and  $E$  curves have been rescaled as indicated. For 3+1D  $SU(3)$  at  $\beta = 6.0$ ,  $V = 16^3 \times 36$ .